Supplementary material for 'The Mars Science Laboratory record of optical depth measurements via solar imaging.'

M.T. Lemmon [a *], S.D. Guzewich [b], J.M. Battalio [c], M.C. Malin [d], A. Vicente-Retortillo [e], M.-P. Zorzano [e], J. Martín-Torres [f g], R. Sullivan [h], J.N. Maki [i], M.D. Smith [j], J.F. Bell III [k],.

[a] Space Science Institute, 4765 Walnut St, Suite B, Boulder, CO 80301, USA.

[b] NASA Goddard Space Flight Center, 8800 Greenbelt Rd, Greenbelt, MD 20771, USA.

[c] Department of Earth and Planetary Sciences, Yale University, 210 Whitney Ave. New Haven, CT 06511, USA.

[d] Malin Space Science Systems, Inc., P. O. Box 910148, San Diego, CA 92121, USA

[e] Centro de Astrobiología (CAB), CSIC-INTA, 28850 Torrejón de Ardoz, Madrid, Spain.

[f] Department of Planetary Sciences, School of Geosciences, University of Aberdeen, Aberdeen AB24 3UE, UK.

[g] Instituto Andaluz de Ciencias de la Tierra (CSIC-UGR), 18100 Armilla, Granada, Spain.

[h] Cornell University, Ithaca, NY, USA.

[j] NASA Goddard Space Flight Center, Greenbelt, MD, USA.

[k] Arizona State University, Tempe, AZ, USA

[i] Jet Propulsion Laboratory, California Institute of Technology, Pasadena, CA, USA

Sand in the baffle: Routine optical depth monitoring showed anomalous increases in M-100 optical depth measurements shortly after sol 1570. Most data remained nominal, with low blue-red differences. However, midsol measurements resulted in increasing differences (Fig. S1). These differences started as several tenths (0.3 in the earliest known example on sol 1576) but increased to >1.5. Based on a comparison with nearby data, some M-34 data were affected, with a peak anomaly of about 0.3. Figure S2 shows the optical depth difference versus elevation angle, demonstrating that the effect had a threshold near 70° elevation. There was no physical basis for the atmospheric optical depth to vary this way: it would require a selective blue absorber or a significant increase in Rayleigh scattering optical depth that happened only near

noon, briefly and repeatedly, without a known cause. Sky images using stereo filters (paired filters at the same wavelength in each camera) taken over sols 1620 to 1626 showed that the obscuration was indeed camera-dependent, not wavelength-dependent. Thus, the obscuration was determined to be in or near the M-100.

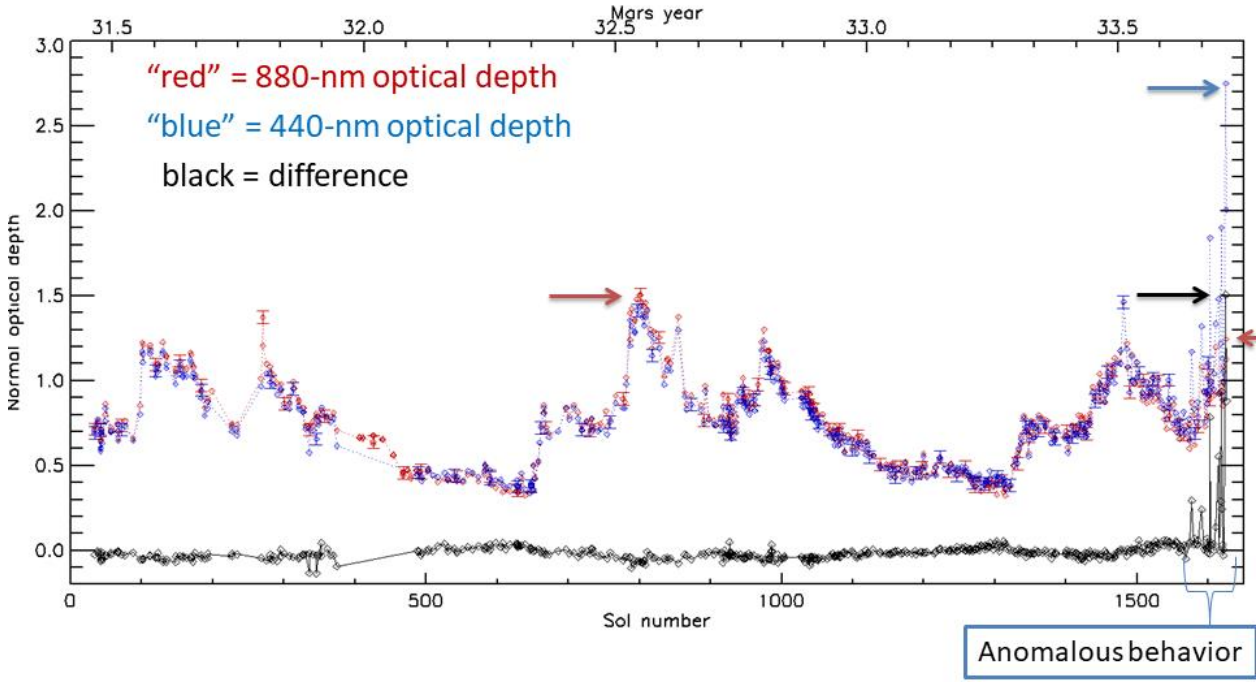

Figure S1. Contemporaneous optical depth retrieval through sol 1625. Arrows indicate peak anomalous blue, red, and difference optical depths from sol 1624 (blue, red, and black, respectively) and the previous peak optical depth of the mission (red).

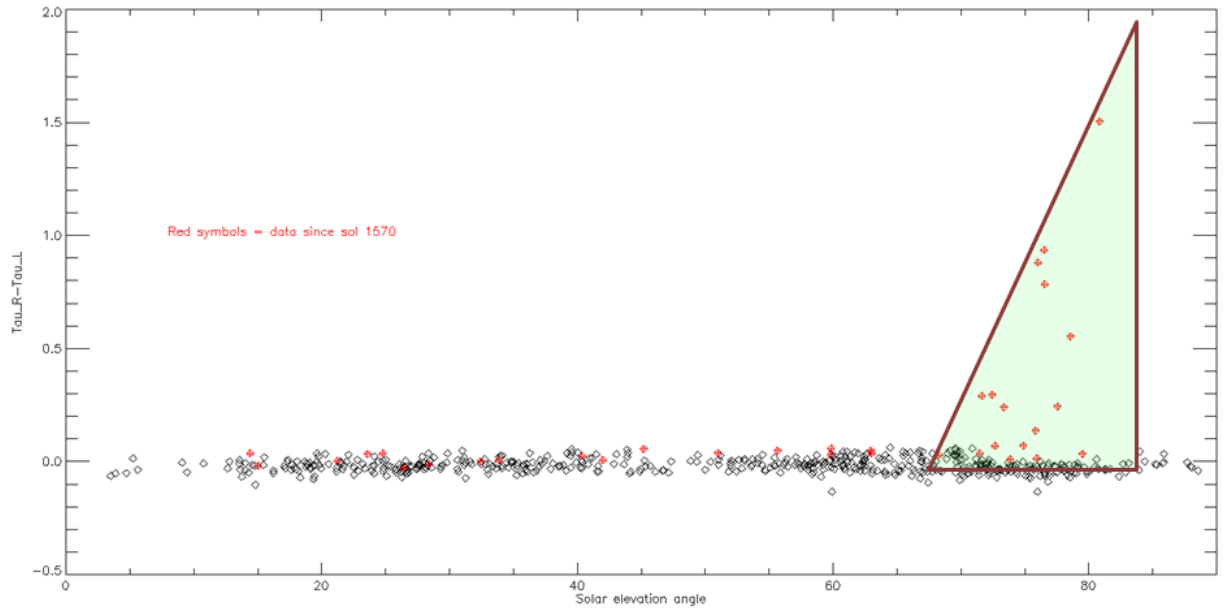

Figure S2. Solar elevation angle dependence. Blue - red (Right - Left) optical depth difference is shown as diamonds, with red diamonds indicating values from sol 1570-1625. The shaded triangle highlights the angles for which the anomaly was seen.

The first detailed characterization was a sky mosaic on sol 1634, taken by aiming at the horizon and panning upward in 5° steps to the zenith and then panning back down (Fig. S3). The upward images showed a dramatic drop in radiance-on-sensor starting at 85° elevation for the M-34 and 70° for the M-100. The downward images showed the brightness increase between 55 and 40° elevation. Our interpretation was that sand increasingly cascaded across the window at the front of the camera as the camera pointed up and then did not mobilize again until there was a significant downward tilt. The piling of sand toward the bottom of the window can also be seen in the radiance profiles (the cameras were at the focus home position, resulting in an out-of-focus horizon, but the window was still far from in-focus). Figure S4 shows the spatial context for the anomaly—the rover was in the process of crossing Bagnold Dunes and was in the immediate area of several sand ripples.

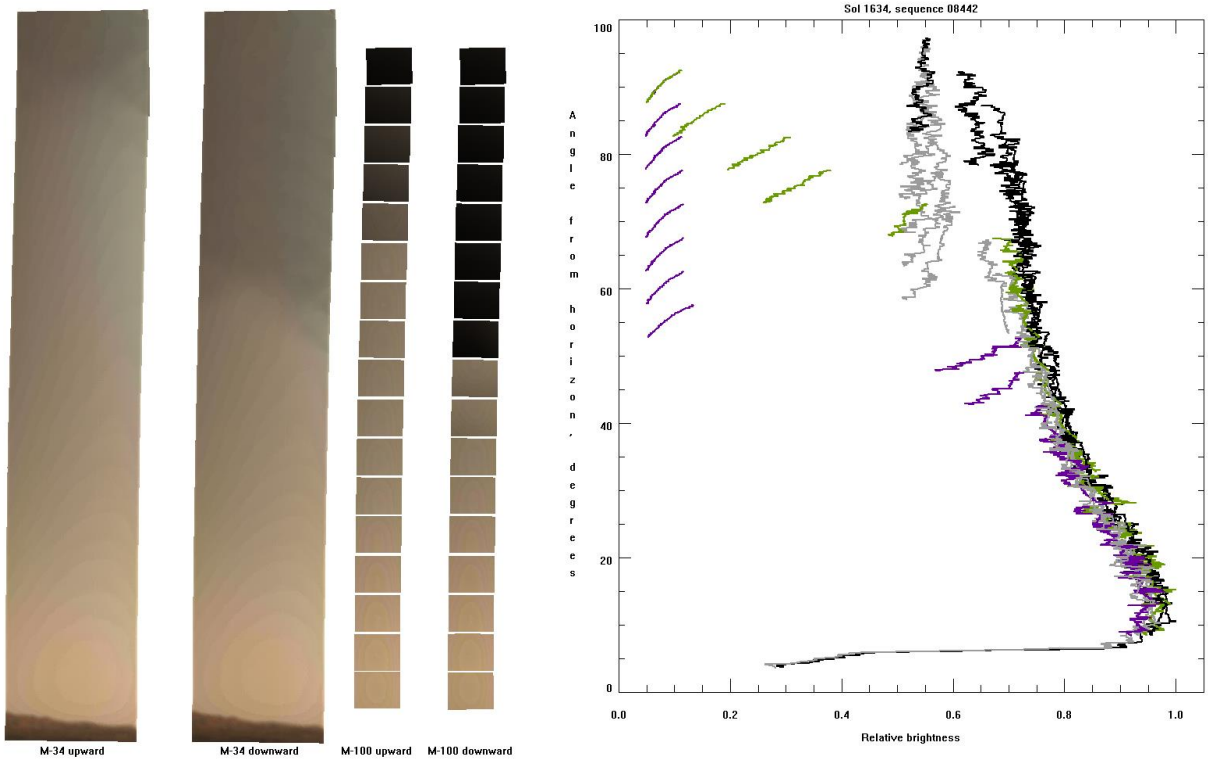

Figure S3. Sky column stereo mosaic. A 17-image column mosaic was taken while panning upward (far left and third from left) and repeated downward (second and fourth from left). Note that each mosaic covers the same sky and is separated to show the hysteresis. On the right, the radiance profiles of the central column of both cameras are shown (black for M-34-upward, gray for M-34-downward, green for M-100 upward, and magenta for M-100-downward).

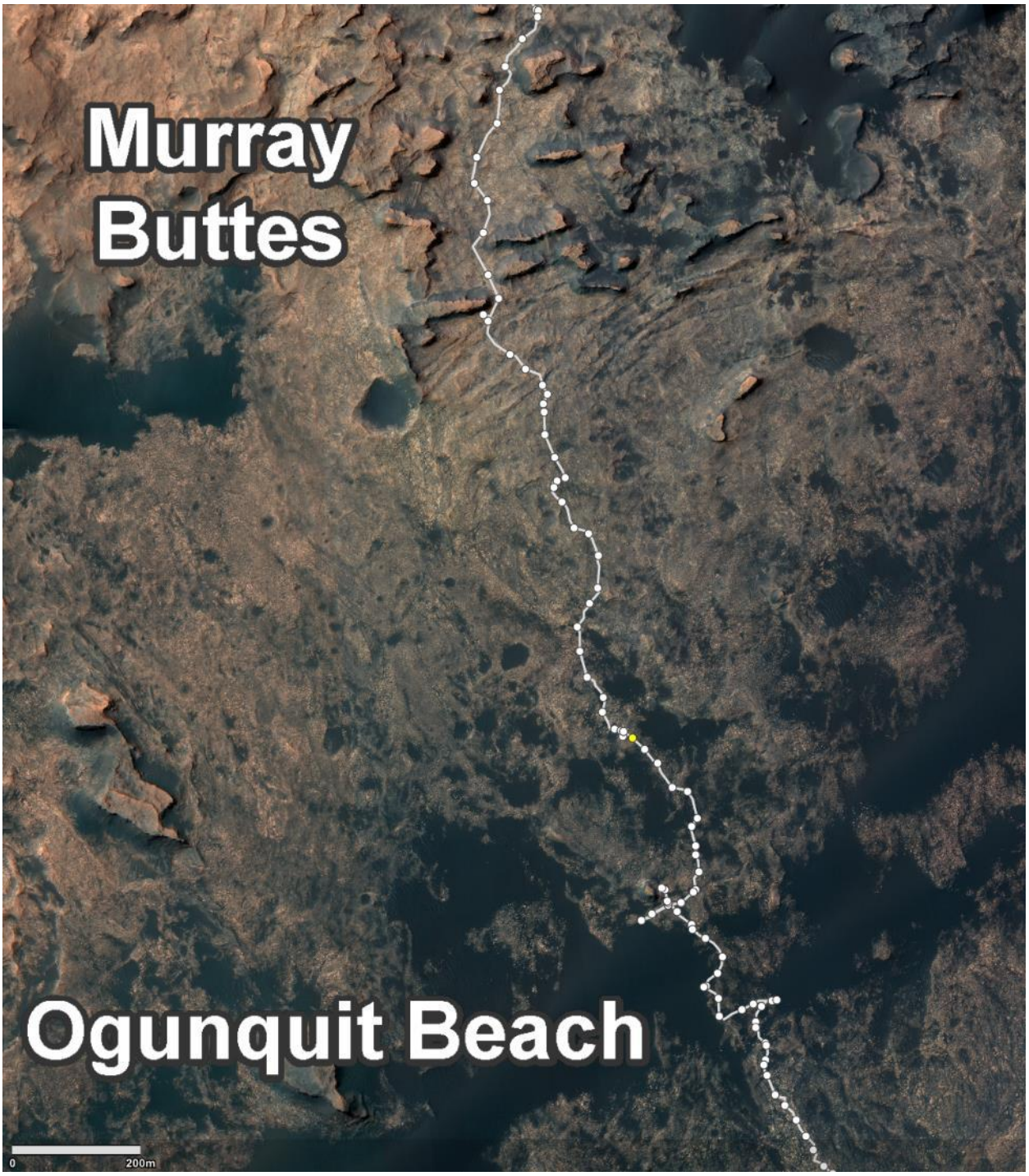

Figure S4. Map of the *Curiosity* traverse. Circles indicate end-of-drive locations for one or more sols. The yellow circle shows the sol-1571 location, while the top and bottom circles of the map correspond to sols 1414 and 1684. Background image[i] credit: NASA/Caltech-JPL.

Saltating sand must have reached 1.9-2.0 m above the surface to get into the baffle, depending on the camera's aim. As illustrated in Fig. S5, a level aim puts the baffle openings 1.97 m above the surface [Malin et al., 2017]. The cameras cannot aim at the nadir, and the 'stow' position was at -45°. Driving with cameras aimed down could limit sand accumulation but did not remove all sand. Searches of past data found low-elevation aims in a Mastcam mosaic on sol 1197, in which sand was seen on the deck where it could have been dumped from the baffles. Downward aims of -72° were a part of right-side wheel imaging on sol 1591 and many times before and since (every ~50 sols).

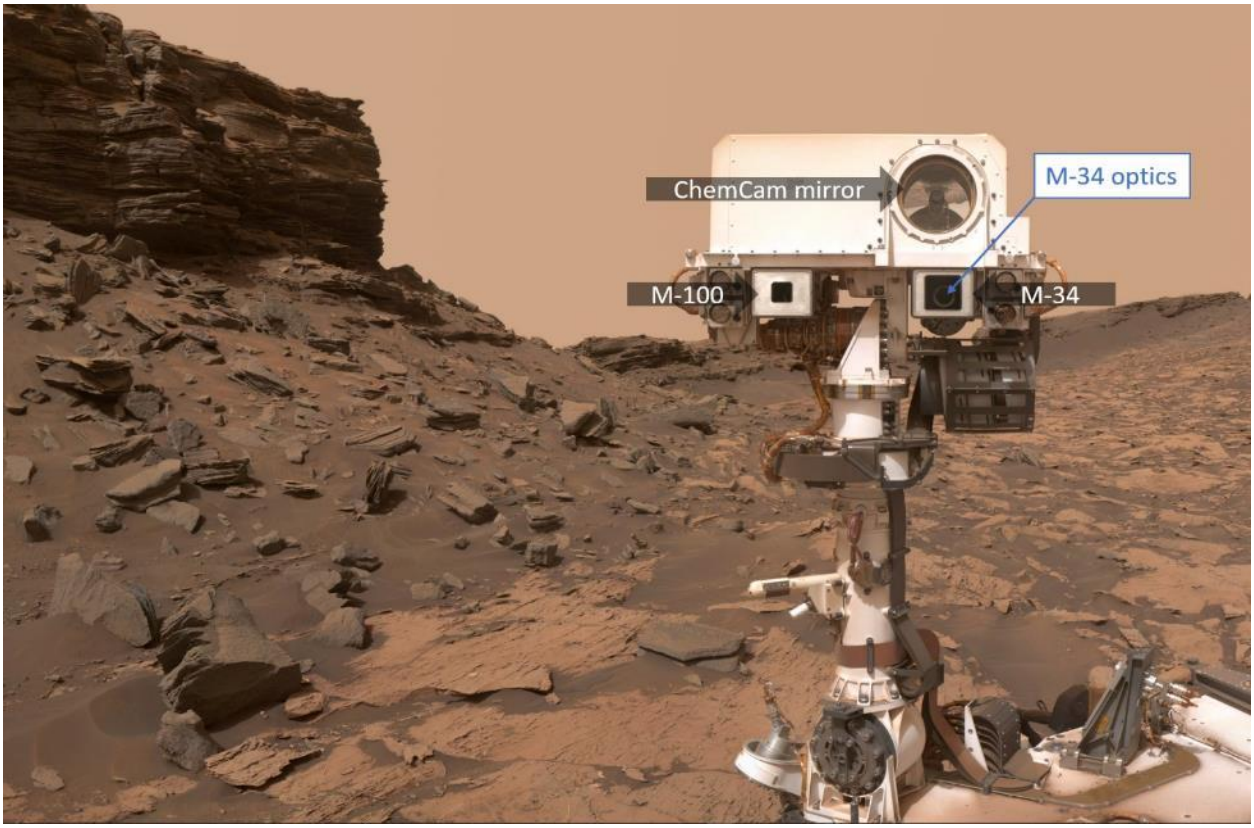

Figure S5: Remote Sensing Mast instruments as seen in a cropped mosaic from MAHLI (Mars Hand Lens Imager) "selfie" on sol 1463 in the Murray Buttes. The M-100 and M-34 baffles are annotated, and the M-34 optics can be seen. From image Planetary Photojournal PIA20844, credit: NASA/JPL-Caltech/MSSS.

After the sand was identified, low aims were tested for sand removal with limited success—the accumulated sand did not increase above the sol-1634 level, but it was not substantially reduced in M-100. The sky column was repeated 33 times and showed variable levels of obscuration. The top aim's mean transmission was tracked and shown in Fig. S6.

M-34 was kept relatively clean. Sand accumulation exceeded removal often enough during southern summer (and in spring, for one instance) that sand presence was sometimes detected. For L_S 0-200°, signs of sand in the baffle were never seen for M-34.

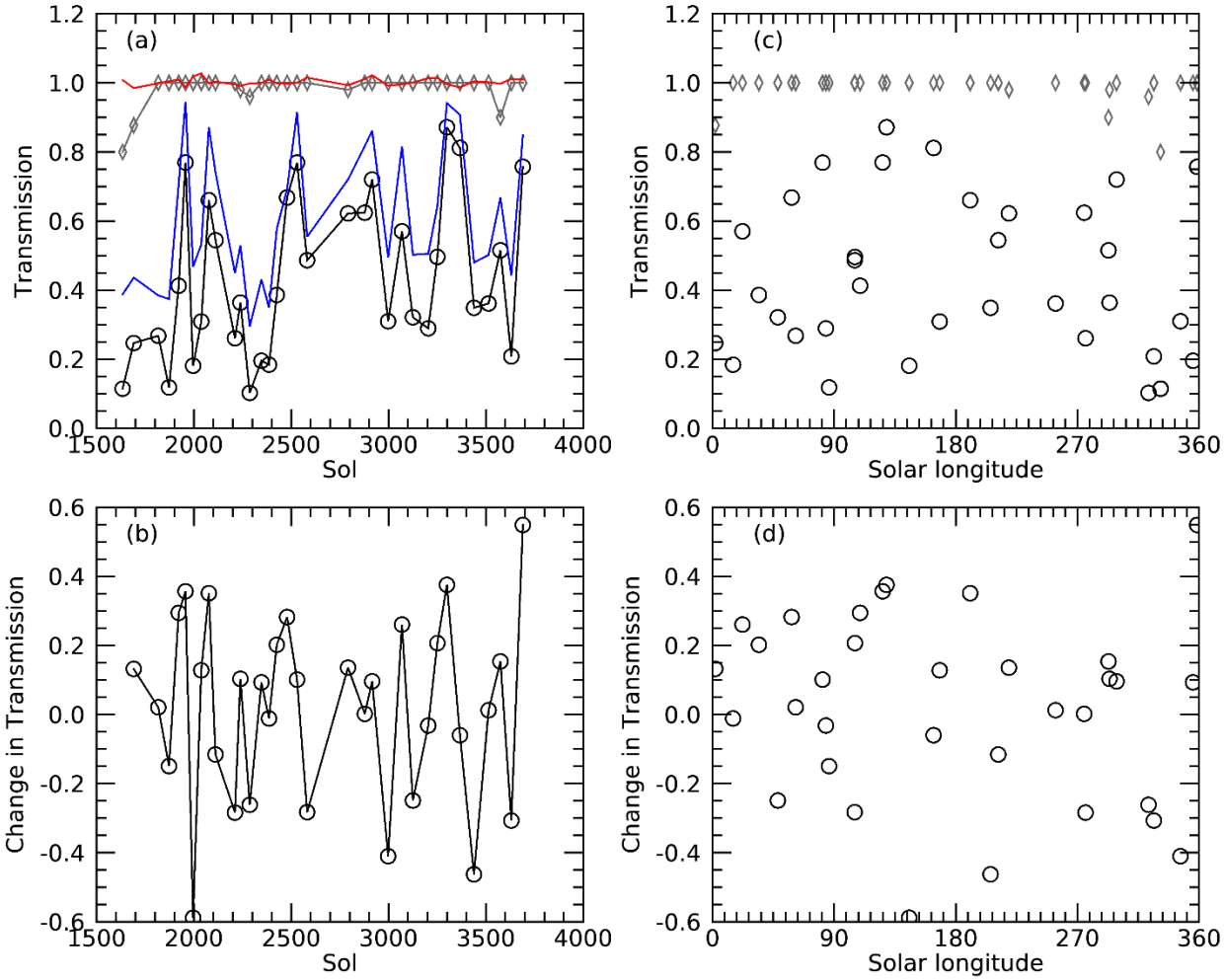

Figure S6: (a) Mean transmission for the M-34 (diamonds) and M-100 (circles) zenith aims. Mean transmission for three M-100 aims around 50° on the upward (red) and downward (blue) scans are shown. (b) The change in mean transmission from its previous value is shown for the M-100 zenith aim. The transmission (c) and transmission change (d) are compared to solar longitude.

M-100 was never wholly cleaned, nor did it ever show more obscuration. Changes in obscuration were consistent with randomness: the measurement uncertainty was about a percent, but the variation in the amount of transmission was unpredictable. The most likely explanation is that a rough equilibrium was established near the maximum capacity for the M-100 when it is aimed down frequently. The amount of sand varied by some unknown amount as accumulation varied, and the pattern of use of the camera dumped sand unpredictably. The amount of sand on the window when the camera was zenith-aimed varied based on sand volume and the aiming details.

That is, the outcome was likely path-dependent: when aimed down, sand would accumulate only in the front of the baffle; when in normal use, the sand would distribute over the bottom; as the camera tipped up, sand would cascade toward the optics, but faced many obstacles that would accumulate some sand; and the amount of sand that finally ended up on the window may have depended on the amount of shaking (e.g., from varying azimuth actuation) while moving up in elevation.

On sol 1629, a two-position multispectral sequence imaged the sky at a low elevation and near the zenith to determine the wavelength variation of transmission (Fig. S7). For the stereo-filter wavelengths (480, 553, and 639 nm in the clear filter, 446, 553, and 1013 nm) the transmission spectrum was directly measured using the right/left comparison. For the other three right-eye filters (805, 908, and 937 nm), the transmission spectrum was estimated by interpolating sky radiance from nearby the left-eye filters. The resulting spectrum was consistent with dark, spectrally neutral sand. However, some contribution from intermixed red dust may cause a slight red slope (0.003%/100-nm).

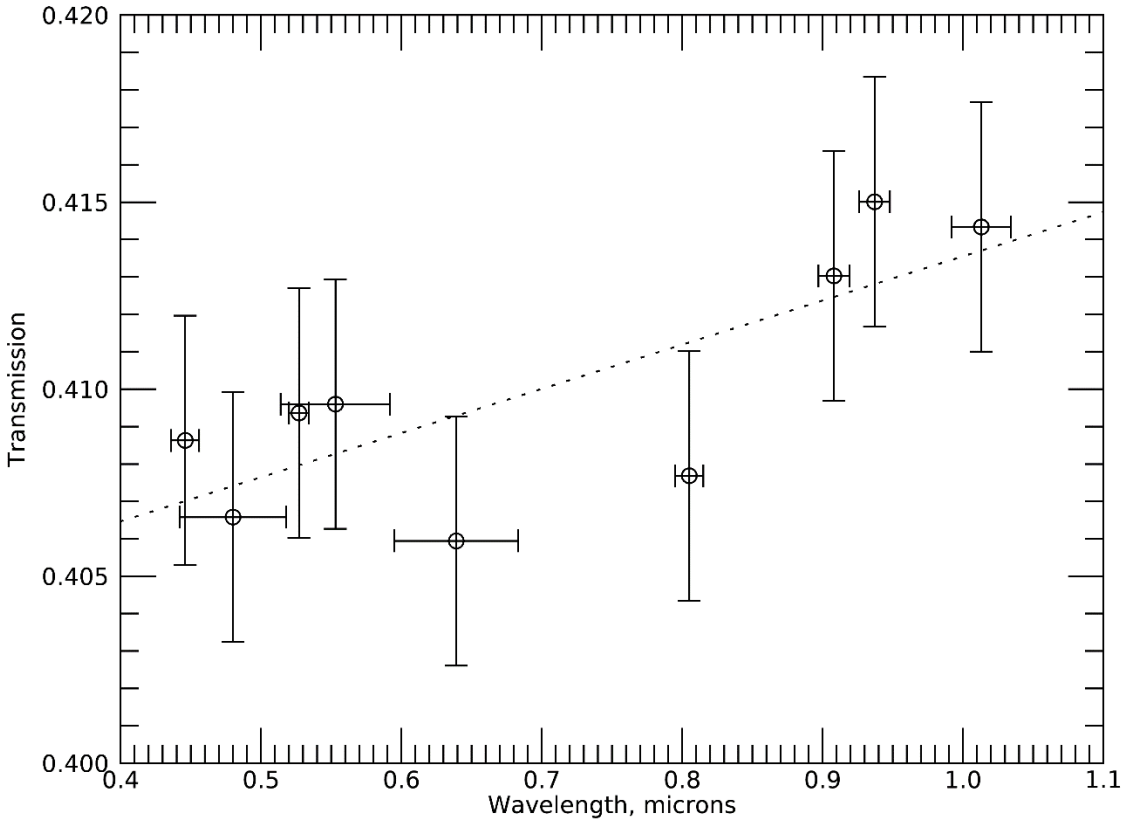

Figure S7. Transmission spectrum from sol 1629.

There is indirect evidence that the grains in the baffle are similar in size to those in ripples, which had median sizes in the 100- to 150-μm range (see main text, section 4.6, for references). Using the methods of Sullivan and Kok [2017], we modeled trajectories for 150-, 200-, and 250-μm grains and found that they can reach the camera height when bouncing over hard ground (Fig. S8). Further, sol-1741 images of sand grains on the rover's deck showed that most grains were <200 μm (Fig. S9).

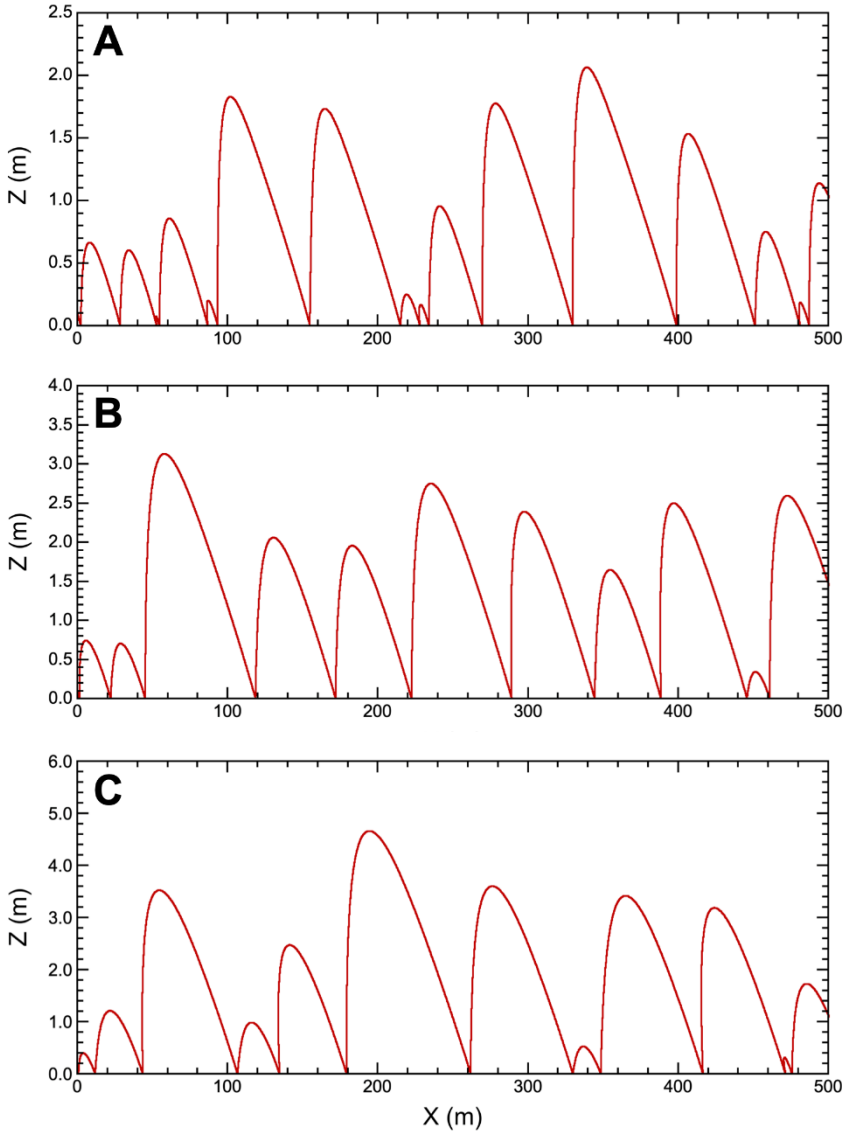

Figure S8. Numerically modelled martian saltation trajectories (Grainwind.c, Sullivan and Kok [2017]) for (A) 150 μm grains, (B) 200 μm grains, and (C) 250 μm grains bouncing over hard ground with wind friction speed u_* = 1 m/s and surface roughness z_0 = 0.0001 m (equivalent to a wind speed u ~25 m/s at height z ~2 m). Other test conditions: atmospheric pressure = 6.7 mb, grain density = 3000 kg/m^3, hard rock bounce factors randomized between 0.5-0.8, and bounce angles were also randomized. In all three cases saltating grains reach the ~2 m height of the MSL camera baffles.

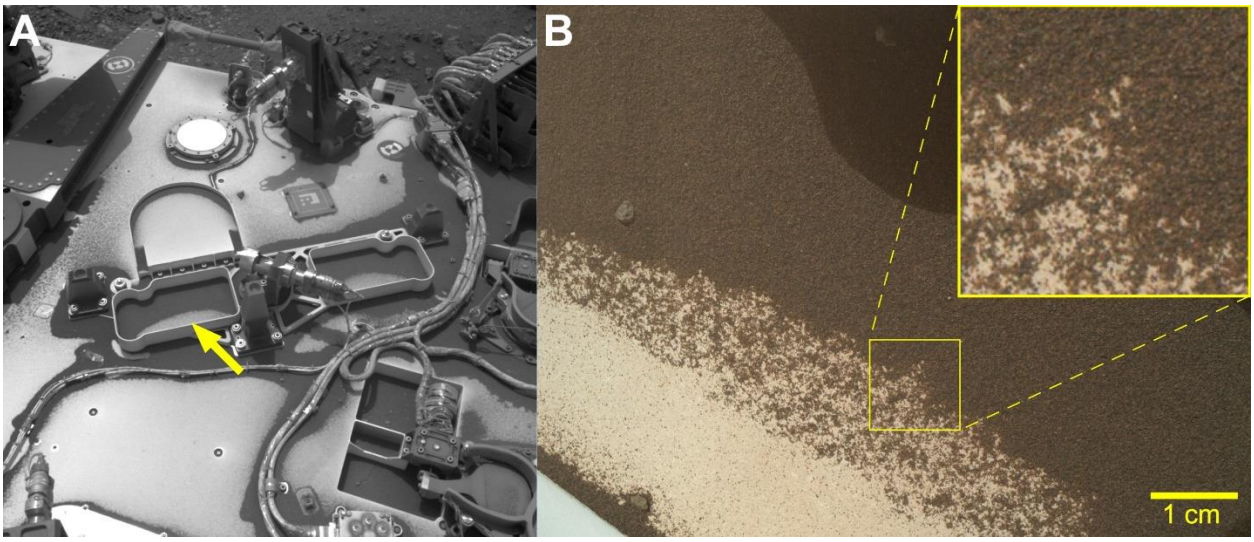

Figure S9. The MSL rover deck includes trays that protected the camera optics on the Remote Science Mast (RSM) while the RSM was still stowed and folded down across the deck. The RSM was raised into position after landing, leaving the protective deck trays empty and open to accumulation of sand, silt, and dust. Grain sizes of particles saltating above the rover deck were constrained by hand-lens quality MAHLI images acquired on sol 1741 of sand grains in one of these deck trays. (A) Brightness-stretched Navcam (Maki et al., 2012) image of the rover deck, including the deck tray imaged by the arm-mounted MAHLI camera. Yellow arrow shows the approximate orientation of the MAHLI view. (Navcam NLA_593685292RAD_F0722464NCAM00101M1.) (B) Color-stretched 52 μm/pixel MAHLI focus-merge image that barely resolves some sand grains in the deck tray. Representative inset shows that the overwhelming majority of grains subtend 4 pixels or less, so they are ≤200 μm. (MAHLI image 1741MH0002580000700207R00.)

References

Maki, J., D. Thiessen, A. Pourangi, P. Kobzeff, T. Litwin, L. Scherr, S. Elliott, A. Dingizian, and M. Maimone (2012) The Mars Science Laboratory engineering cameras, *Space Science Reviews*, *170*, 77–93, https://doi.org/10.1007/s11214-012-9882-4

[i] https://mars.nasa.gov/maps/location/?mission=MSL&site=MBT&mapLon=137.36429214477542&mapLat=-4.700835354237159&mapZoom=15&globeLon=137.3978687&globeLat=-4.663687049999997&globeZoom=13&globeCamera=0,-2441.40625,0,0,1,0&panePercents=0,100,0&on=Current Position$1.00,Waypoints$1.00,Surface View$1.00,Rover Path$1.00,Labels$1.00,Basemap$1.00,Gale Crater Map$1.00